Toxicology in Vitro 65 (2020) 104814

Contents lists available at ScienceDirect

Toxicology in Vitro

journal homepage: www.elsevier.com/locate/toxinvit

Novel benzoate-lipophilic cations selectively induce cell death in human colorectal cancer cell lines

José Antonio Jara[a], Diego Rojas[b], Vicente Castro-Castillo[c], Sebastián Fuentes-Retamal[b], Cristian Sandoval-Acuña[b], Eduardo Parra[d], Mario Pavani[b], Juan Diego Maya[b], Jorge Ferreira[b,*], Mabel Catalán[b,*]

[a] Institute for Research in Dental Sciences (ICOD), Faculty of Dentistry, Universidad de Chile, Santiago, Chile
[b] Clinical and Molecular Pharmacology Program, Institute of Biomedical Sciences (ICBM), Faculty of Medicine, Universidad de Chile, Santiago, Chile
[c] Department of Physical Chemistry and Chemistry, Faculty of Chemical and Pharmaceutical Sciences, Universidad de Chile, Santiago, Chile
[d] School of Medicine, Faculty of Health Sciences, University of Tarapacá, Av. General Velásquez 1775, Arica 1000007, Chile

ARTICLE INFO

Keywords:
Targeting mitochondria
Benzoic acid derivatives
Uncoupling agents
Metabolism stress
Triphenylphosphonium moiety
Colorectal cancer
Antitumour-mitochondrial agents

ABSTRACT

Introduction: Colorectal cancer (CRC) is a critical health issue worldwide. The high rate of liver and lung metastasis associated with CRC creates a significant barrier to effective and efficient therapy. Tumour cells, including CRC cells, have metabolic alterations, such as high levels of glycolytic activity, increased cell proliferation and invasiveness, and chemo- and radio-resistance. However, the abnormally elevated mitochondrial transmembrane potential of these cells also provides an opportunity to develop drugs that selectively target the mitochondrial functions of tumour cells.

Methods: In this work, we used a new batch of benzoic acid esters with cytotoxic activities attached to the triphenylphosphonium group as a vehicle to target tumour mitochondria and improve their activity. We evaluated the cytotoxicity, selectivity, and mechanism of action of these derivatives, including the effects on energy stress-induced apoptosis and metabolic behaviour in the human CRC cell lines HCT-15 and COLO-205.

Results: The benzoic acid derivatives selectively targeted the tumour cells with high potency and efficacy. The derivatives induced the uncoupling of the oxidative phosphorylation system, decreased the transmembrane potential, and reduced ATP levels while increasing AMPK activation, thereby triggering tumour cell apoptosis in both tumour cell lines tested.

Conclusion: The benzoic acid derivatives studied here are promising candidates for assessing in vivo models of CRC, despite the diverse metabolic characteristics of these tumour cells.

1. Introduction

Colorectal cancer (CRC) is one of the most common cancers worldwide, causing approximately 700,000 deaths annually and representing a significant burden of disease. In Chile, CRC prevalence is on the rise, accounting for almost 20% of cancer deaths during 2009 (Okada et al., 2016). The complete resection of the primary tumour is often a curative CRC treatment if it is detected early. However, in advanced stages, adjuvant chemotherapy is usually required to prevent local recurrence and metastasis. Few conventional chemotherapy drugs are available to treat CRC, all of which have drawbacks, including drug resistance, loss of efficacy, and numerous side effects (Granci et al., 2013). Furthermore, monoclonal antibodies for specific targets are useful in only a portion of the CRC population, and numerous drug resistance mechanisms have been reported for these therapies (Khelwatty et al., 2015; Mirone et al., 2016) and have high associated costs.

Tumour cells exhibit profound metabolic alterations, such as high glucose uptake, high ATP production through glycolysis at normal oxygen concentrations and the generation of large quantities of lactate (Pavlova and Thompson, 2016; Warburg et al., 1927). This metabolic shift towards a glycolytic profile confers bioenergy and biosynthetic advantages to proliferating cancer cells by increasing the non-oxidative ATP production and generating intermediate glucose metabolites that are routed to the tumour cells for biosynthetic processes (Zhang et al., 2015). Therefore, mitochondrial function is also altered in cancer cells.

* Corresponding authors at: Clinical and Molecular Pharmacology Program, Institute of Biomedical Sciences (ICBM), Faculty of Medicine, Universidad de Chile, Independencia 1027, Santiago, Chile.
E-mail addresses: jferreir@med.uchile.cl (J. Ferreira), mabelcatalan@med.uchile.cl (M. Catalán).

https://doi.org/10.1016/j.tiv.2020.104814
Received 16 October 2019; Received in revised form 1 February 2020; Accepted 25 February 2020
Available online 27 February 2020

Cancer cells have a significantly more negative mitochondrial transmembrane potential (ΔΨm), a lower respiration rate, and a lower mitochondrial mass than normal cells (Hoye et al., 2008; Moreno-Sanchez et al., 2007; Ralph and Neuzil, 2009). This metabolic reprogramming facilitates tumour cell proliferation, invasiveness, and chemo- and radio-resistance (Wahdan-Alaswad et al., 2013).

The differences between normal cell and tumour cell mitochondria provide a chemical opportunity to selectively target this organelle. Given the mitochondrial hyperpolarization of cancer cells, positively charged lipophilic molecules can be designed to accumulate within the mitochondria (Kalyanaraman et al., 2017; Neuzil et al., 2013; Reily et al., 2013).

In addition, the triphenylphosphonium (TPP^+) moiety can be used to enhance the transport of molecules into the mitochondria (Murphy, 2008; Yang et al., 2016). Moreover, the TPP^+ moiety has been added to various pharmacologically active groups to produce new compounds intended to target cancer cell mitochondria. These compounds have been found to show remarkable cytotoxic activity in cancer cell lines, as well as anti-tumour effects in vivo (Millard et al., 2010; Rokitskaya et al., 2016; Yasui et al., 2017).

Recently, our group described several new gallic acid (GA) derivatives linked to the TPP^+ moiety through an aliphatic chain. These GA derivatives had a cytotoxic effect, triggered apoptosis in vitro, and showed an antitumoural effect in vivo in a murine carcinoma model (Jara et al., 2014; Peredo-Silva et al., 2017).

This work expands upon these discoveries by evaluating the cytotoxicity and modes of action of a new set of benzoic acid esters linked to TPP^+ (benzoate-TPP^+ compounds) in colorectal cancer cell lines, including the effects on metastatic and drug-resistant behaviours.

2. Materials and methods

2.1. Materials

Roswell Park Memorial Institute (RPMI) 1640 culture medium, FCCP (carbonyl cyanide 4-(trifluoromethoxy)phenylhydrazone), glutamine, glucose, MTT, DMSO, foetal bovine serum (FBS), and Trypan Blue 0.4% solution were purchased from Sigma Chemical Co. (St. Louis, MO). Minimum Essential Medium (MEM) with Earle's Balanced Salts (MEM/EBSS), penicillin/streptomycin, and trypsin were purchased from HyClone Laboratories (South Logan, UT). All other organic compounds and inorganic salts, acids, and solvents were purchased from Merck (Darmstadt, Germany). The primary antibodies for AMPK-P, AMPK-T, and β-actin were purchased from Cell Signaling Technologies (Boston, MA).

2.2. Synthesis of benzoate-TPP^+ derivatives

Benzoate-TPP^+ derivatives were synthesized and characterized as previously described (Sandoval-Acuna et al., 2016). In detail, the first step consisted in the synthesis of (10-hydroxydecyl)triphenylphosphonium bromide performed as follows: A solution of 10-bromodecan-1-ol in dry acetonitrile (100 mL) was treated with triphenylphosphine. The solution was refluxed with stirring for 48 h. The solvent was removed in a vacuum pump, and the crude product was subjected to chromatography on silica gel (EtOAc, MeOH) to yield (10-hydroxydecyl)triphenylphosphonium bromide as a colorless oil (63%). ^{1}H NMR (400 MHz, DMSO-d_6): δ 1.01–1.51 (m, 18H, CH2), 3.57 (t, J = 7.1 Hz, 2H, CH2), 7.73–7.91 (m, 15H, ArH). HRMS: m/z 485.4312 (calcd for C27H33BrOP 485.4357). The second step involved a Steglich esterification, using N,N-dicyclohexylcarbodiimide (DCC) as reagent, 4-Dimethylaminopyridine (DMAP) as catalyst and N,N- dimethylformamide (DMF) as solvent. Briefly, in an atmosphere of N2, a solution of each respective hydroxybenzoic acid in dry DMF was treated with a solution of DCC in dry DMF. The mixture was cooled to 0 °C, and a solution of (10-hydroxydecyl) triphenylphosphonium bromide and DMAP in DMF was added. The reaction was stopped the next day, and any resulting precipitate was removed by filtering. The solvent was then removed, producing a residue that was subjected to chromatography on silica gel (DCM, MeOH). Fig. S1 showed the benzoate-TPP^+C_{10} derivatives chemical characterization.

2.3. Cell lines and cultures

The human colon cancer cell lines HCT-15 and COLO 205 and the normal colon epithelial cell line CCD841 CoN were acquired from the American Type Culture Collection (ATCC). Cells were amplified from passages 0 to 10 and kept in liquid nitrogen until use. Colon cancer cells were grown in RPMI 1640 medium. CCD 841 CoN cells were grown in MEM/EBSS. All cells were supplemented with 10% FBS, 100 U/mL penicillin, and 100 μg/mL streptomycin in a humidified 5% CO_2 / 95% air atmosphere at 37 °C. For passages (no more than 20), cells were detached using trypsin and seeded in plates for the various experiments.

2.4. MTT cell viability

Cells were seeded into 96-well plates (1×10^4 per well). After 24 h, the benzoate-TPP^+ compounds were added in increasing concentrations. Cells were incubated for 24, 48, or 72 h. After incubation, cells were washed twice with PBS, and 100 μL of 0.5 mg/mL MTT solution was added to each well. After 2 h of incubation for the CRC cell lines and 4 h for the normal cell line (as additional time is required to generate formazan crystals in normal vs. tumour cell lines), the MTT was removed and the formazan crystals were dissolved in 50 μL of DMSO per well. The absorbance was measured at 570 nm using a microplate ELISA reader (Bio-Rad, Hercules, CA).

2.5. Oxygen consumption and extracellular acidification rates

The oxygen consumption rates (OCR) of the COLO 205 and HCT-15 cell lines were measured polarographically using Clark electrodes (Yellow Spring Instruments Co. Ohio, USa), as described previously (Cordano et al., 2002; Plaza et al., 2008). The extracellular acidification rate was measured using pH electrodes (Cole-Palmer, IL, USA), as described previously. CRC cells were cultured at 80% confluence. The cells were trypsinized and counted using 7×10^6 cells from the HCT-15 cell line and 4×10^6 cells from the COLO 205 cell line for each analysis. Briefly, 0.6 mL of cell suspension in medium consisting of 150 mM NaCl, 5 mM KCl, and 1 mM Tris hydrochloride pH 7.0 along with 4 mM glutamine and 5 mM glucose as substrates were added to the chamber containing the electrodes. For basal measurements, respiration and H^+ release rates were measured in the presence of substrates until complete oxygen consumption was achieved (anoxia). The respiration rate was inhibited with 1 μg/mL oligomycin. OXPHOS was fully uncoupled with 0.155 μM FCCP as a control. OCR and H^+ release rates were evaluated by adding increasing concentrations of each benzoate-TPP^+ compound. The results were normalized to OCR in the presence of oligomycin and compared with the effects of FCCP. Data analysis was performed using SigmaPlot 12 (San Jose, CA, USA).

2.6. Mitochondrial mass

To measure mitochondrial mass, 100 nM MitoTracker Green FM solution in RPMI 1640 medium without FBS was prepared. Detached cells (1×10^5) were deposited in a 1.5-mL Eppendorf tube with 100 μL of 100 nM MitoTracker Green FM solution and incubated for 45 min. The cells were centrifuged, and the pellets were washed with PBS. After another centrifugation, the cell pellets were resuspended in FBS-free medium. Cells were analysed using Flow Cytometry FACS (FACS Aria® III, BD Biosciences) at a wavelength of 490 nm Ex/516 nm Em.

2.7. Intracellular ATP levels

Intracellular ATP levels were measured using the CellTiter-Glo Luminescent Assay (Promega, Madison, WI) according to the manufacturer's protocol. Cells were seeded in 96-well plates (1×10^4 cells per well) and incubated for 24 h. Each well was stimulated with benzoate-TPP^+ compounds at the given concentrations for 4 h. Next, an aliquot of the cell suspension was transferred to an opaque 96-well plate and maintained in the dark at room temperature for 10 min. Luminescence was measured using a Thermo Scientific Varioskan Flash spectral scanning multimode reader.

2.8. AMPK-P/AMPK-T western blot analysis

Cells were treated with benzoate-TPP^+ compounds for 4 h and then washed in cold PBS and lysed with 40 × −diluted RIPA buffer (50 mM Tris-HCl; 150 mM NaCl; 0.1% sodium dodecyl sulfate) containing a proteinase and phosphatase inhibitor cocktail (Cell Signaling Technologies, Boston, MA). A 40 μg sample of each protein was separated by 10% SDS-polyacrylamide gel electrophoresis (SDS-PAGE), and the resolved proteins were transferred to a methylcellulose membrane (Millipore, Billerica, MA). The membranes were blocked with 5% nonfat milk in Tris-buffered saline with 0.1% Tween-20 at room temperature for 1 h and then incubated with the primary antibody for AMPK-P (dilution 1:1000), AMPK-T (dilution 1:1000), or β-actin (dilution 1:1000) at 4 °C overnight. Membranes were washed and then incubated with anti-rabbit horseradish peroxidase-conjugated secondary antibody for 2 h at room temperature (dilution 1:5000). After washing, the membranes were exposed to an enhanced chemiluminescent reagent (EZ-ECL). A ChemiDoc MP System was used for Western blotting. Digital blots were quantified using ImageJ software.

2.9. Changes in mitochondrial transmembrane potential

Changes in the transmembrane potential (ΔΨm) were determined using tetramethyl rhodamine methyl ester (TMRM) as a probe. Cells were seeded into 24-well plates (1×10^5 cells per well) for 24 h and then incubated with 200 nM TMRM probe. Cells were immediately exposed to increasing concentrations of each compound (2.5 to 30 μM) for 30 min. After washing with PBS, cells were detached and resuspended in cold PBS for analysis using flow cytometry FACS (FACSAria® III, BD Biosciences) at a wavelength of 540 nm Ex/595 nm Em.

2.10. Flow cytometry measurement of apoptosis

The apoptotic events induced by the compounds were determined using an Annexin V-FITC Apoptosis Detection Kit (Abcam, Cambridge, MA) according to the manufacturer's protocol. Cells were seeded in 24-well plates (5×10^5 cells per well) for 24 h. Cells were then incubated with various concentrations of the compounds for 48 h. Cells were detached and resuspended in 250 μL of 1× Annexin buffer with 2.5 μL of Annexin V probe and 2.5 μL of propidium iodide for each sample. Finally, cells were incubated for 5 min with the probes, light-protected, and further analysed using flow cytometry (FACS Canto A, BD Biosciences). The laser wavelength used was 488 nm and the emission wavelengths were FITC-A 530 nm for Annexin V and PerCP-Cy5–5-A 617 nm for propidium iodide. A total of 10,000 events per sample were acquired, and the data were analysed using Cyflogic software (non-commercial version, CyFlo Ltd.).

2.11. Caspase 3 activation

Activation of caspase 3 by the compounds was performed using a PE Active Caspase-3 Apoptosis Kit (BD, Franklin Lakes, NJ) according to the manufacturer's protocol. Briefly, cells were seeded in 24-well plates (5×10^5 cells per well) for 24 h. Cells were then incubated with various concentrations of the compounds for 24 h. Cells were detached and resuspended in cell permeability/fixation buffer and incubated for 30 min in the dark at 4 °C. Cells were centrifuged and washed once with cell-staining buffer, centrifuged and resuspended in anti-caspase PE antibody and incubated for 30 min in the dark. Finally, cells were washed once with cell-staining buffer and analysed using flow cytometry at a wavelength of 488 nm Ex/617 nm Em. The data were analysed using Cyflogic software (non-commercial version, CyFlo Ltd.).

2.12. Statistical analysis

The data were analysed using one-way or two-way ANOVA and Bonferroni's or Tukey's post-test. The IC_{50} was calculated using a dose-response curve with a variable slope in GraphPad Prism 6. The differences were considered significant at $p < .05$.

3. Results

3.1. Cytotoxicity and selectivity of benzoate-TPP^+ compounds

In this work, we evaluated a series of lipophilic cations derived from 3,4,5 tri-hydroxybenzoic acid (gallic acid, Fig. S2A) esters with a 10-carbon aliphatic unit coupled to the TPP^+ moiety (TPP^+C_{10}) (Fig. 1A), which were previously synthesized and characterized (Sandoval-Acuna et al., 2016). Fig. 1B and C illustrate the structures of these 2,5-di-hydroxy (GA-TPP^+C_{10}) and 2-hydroxy (SA-TPP^+C_{10}) benzoic acid derivatives. The synthesis of the intermediates was also evaluated as comparative molecules to characterize the TPP^+ effect. The OH-C_{10}, OH-C_{10}GA and OH-C_{10}SA molecules (Fig. S2D, S2E and S2F, respectively) correspond to the esters of benzoic acid without the TPP^+ moiety. Furthermore, the decyl ester (DA-TPP^+) (Fig. S2G) was evaluated to establish the importance of benzoic acid on the cytotoxic effects and was used as a control to characterize these effects.

Cytotoxicity was evaluated in two colorectal cancer cell lines with different tumour behaviours, HCT-15 and COLO 205, derived from a non-metastatic tumour with resistance to standard drug therapy and from a metastatic site, respectively. Fig. 2 shows that the compounds SA-TPP^+C_{10}, GA-TPP^+C_{10}, and TPP^+C_{10} induce a cytotoxic effect in a concentration- and time-dependent manner in both HCT-15 (Fig. 2A, B, and C, respectively) and COLO 205 cell lines (Fig. 2D, E, and F, respectively). Cytotoxicity was quantified by measuring the IC_{50} values of the three compounds in both cell lines. Table 1 shows the IC_{50} values for all compounds at 24, 48, and 72 h. The compounds SA-TPP^+C_{10}, GA-TPP^+C_{10}, and TPP^+C_{10} had IC_{50} values of 5–16 μM at 24 h, 3–14 μM at 48 h, and 3–12 μM at 72 h in both cell lines. All compounds showed similar IC_{50} values at each time point evaluated (Table 1), with no significant difference in terms of cytotoxic activity among any of the compounds. In addition, the cytotoxic effect of the control molecules without the TPP^+ moiety showed limited potency and efficacy, with high IC_{50} values. However, DA-TPP^+ produced a strong, non-selective cytotoxic effect (Table 1; Fig. S3A and S3B).

To measure selectivity, we evaluated the cytotoxicity of the benzoate-TPP^+ compounds in CCD 841 CoN cells, a non-tumour colorectal epithelial cell line, and then calculated the selectivity index by comparing the IC_{50} for non-tumour vs. tumour cells at 48 h and 72 h of incubation. Table 2 shows that GA-TPP^+C_{10} had higher IC_{50} values for CCD 841 CoN than SA-TPP^+C_{10} or TPP^+C_{10}, a selectivity index of 10 for HCT-15 cells and 41 for COLO 205 cells after 48 h, and a selectivity index of 3 for HCT-15 cells and 10 for COLO 205 cells after 72 h (Table 2). These results show decreased viability after exposure to SA-TPP^+C_{10}, GA-TPP^+C_{10}, and TPP^+C_{10}, respectively, with high selectivity for the COLO 205 and HCT-15 cell lines vs. the non-tumour cell line at 48 h. However, at 72 h, the differences were observed between the tumour and non-tumour cell lines for SA-TPP^+C_{10} and GA-TPP^+C_{10}, but not TPP^+C_{10}, suggesting that SA-TPP^+C_{10} and GA-

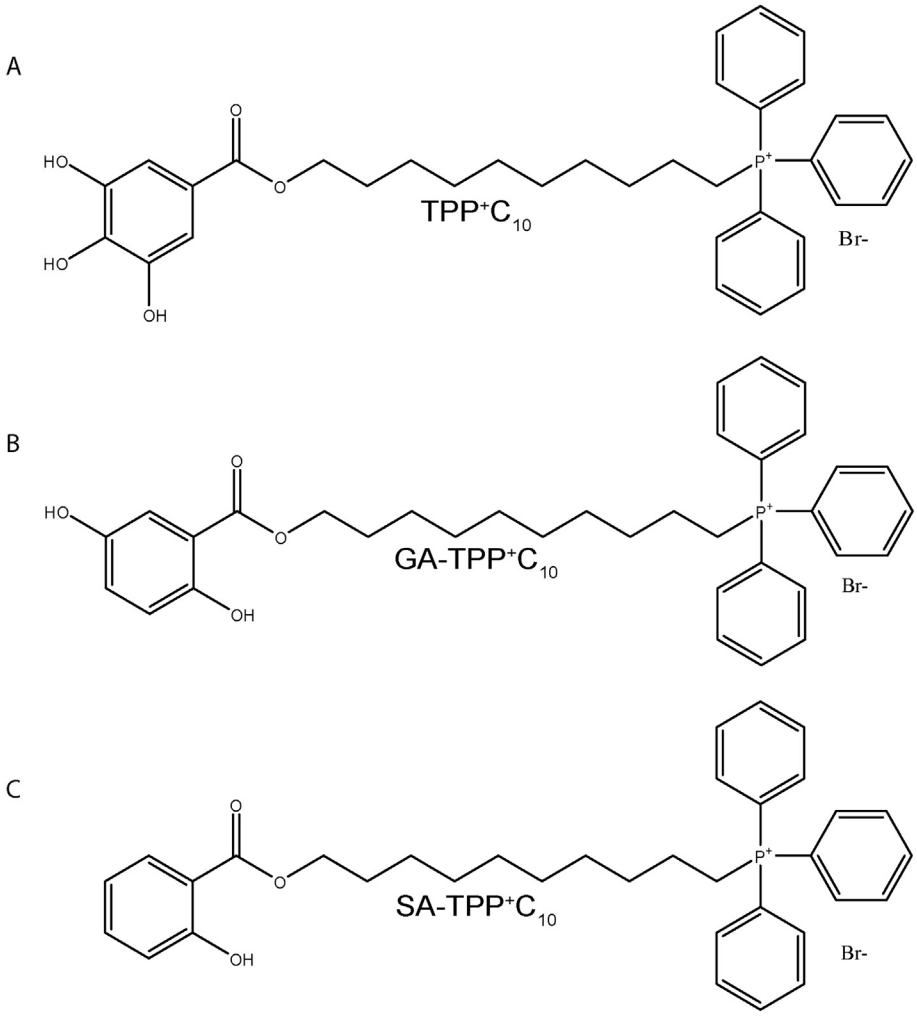

Fig. 1. Structures of benzoate-TPP^+ compounds linked to the triphenylphosphonium moiety (TPP^+), allowing for mitochondrial tropism. Structures were obtained using ChemDraw 9.0 software. A) (10-((3,4,5-trihydroxybenzoyl)oxy)decyl)triphenylphosphonium bromide (TPP^+C_{10}), B) (10-((2,5-dihydroxybenzoyl)oxy)decyl)triphenylphosphonium bromide (GA-TPP^+C_{10}), C) (10-((2-hydroxybenzoyl)oxy)decyl)triphenylphosphonium bromide (SA-TPP^+C_{10}), D) 10-hydroxydecil-3,4,5-trihydroxybenzoate, (OH-C_{10}) E) 10-hydroxydecil-2,5-dihydroxybenzoate (OH-C_{10}GA), F) 10-hydroxydecil-2-hydroxybenzoate (OH-C_{10}SA) and G) decyltriphenylphosphonium bromide ($C_{10}TPP^+$).

TPP^+C_{10} were more selective for tumour cells than TPP^+C_{10}.

Moreover, the results were supported by PI cell incorporation studies (Fig. S2C). We showed that none of the compounds significantly induced cell death, even at 100 μM, which represents a 10- and 40-fold improvement in IC_{50} in HCT-15 and COLO 205, respectively.

3.2. Mechanism of action of benzoate-TPP^+ compounds

Fig. 3A and B show the results for the OCR and media acidification in the basal state. The HCT-15 cells showed a lower OCR than the COLO 205 cells. In contrast, media acidification, as measured by proton release into the medium, was considerably greater in the HCT-15 cells than in the COLO 205 cells. The latter cells only showed increased rates of proton release when the oxygen was depleted.

To evaluate OCR, tumour cells were deposited into the electrode chamber at time zero using oligomycin to inhibit OXPHOS. The compounds or DMSO (as a control) were then added at various concentrations (Fig. 3C). The results were compared with values for the classical uncoupler FCCP. Fig. 3D, E, and F show that in HCT-15 cells, all three compounds increased the oxygen consumption rate (that is, there was an uncoupling effect). SA-TPP^+C_{10} had an uncoupling effect at concentrations above 10 μM, reaching the full uncoupling effect at 50 μM (Fig. 3D). However, while GA-TPP^+C_{10} showed a pattern similar to that of SA-TPP^+C_{10}, this compound did not achieve the full uncoupling effect at any concentration (Fig. 3E). TPP^+C_{10} also induced an uncoupling effect, but this compound was less potent than GA-TPP^+C_{10} or SA-TPP^+C_{10} and failed to achieve the full uncoupling effect at any concentration (Fig. 3F).

The three compounds were also able to exert an uncoupling effect in COLO 205 cells at lower concentrations. SA-TPP^+C_{10} showed a concentration-dependent uncoupling effect at concentrations above 5 μM, reaching the full uncoupling effect at 20 μM (Fig. 3G). GA-TPP^+C_{10} showed the same pattern as SA-TPP^+C_{10}, reaching the full uncoupling effect at 10 μM (Fig. 3H). TPP^+C_{10} produced similar results in the COLO 205 cells as in the HCT-15 cells, showing a concentration-dependent uncoupling of OXPHOS (Fig. 3F and I). This compound was again less potent than GA-TPP^+C_{10} or SA-TPP^+C_{10}, achieving the full uncoupling effect at 30 μM (Fig. 3I).

Fig. 3J and K show the total mitochondrial fluorescence visualized using MitoTracker Green FM. This probe is incorporated into the mitochondria independent of transmembrane potential in tumour and non-tumour cell lines. The results suggest that non-tumour cells (CCD 841 CoN) contain a greater number of mitochondria than COLO 205 or HCT-15 cells.

3.3. Metabolic effects induced by benzoate-TPP^+ compounds

To evaluate the acute consequences induced by the uncoupling effect of benzoate-TPP^+ derivatives, we observed the loss of $\Delta\Psi m$ as an early and critical event that triggers cell death after exposure to an uncoupling agent (Kroemer et al., 2007). All three compounds induced a significant decrease in $\Delta\Psi m$ in both the HCT-15 (Fig. 4A) and COLO 205 (Fig. 4B) cell lines. However, benzoate-TPP^+ derivatives did not produce significant changes in $\Delta\Psi m$ in non-tumour cells (Fig. S4G),

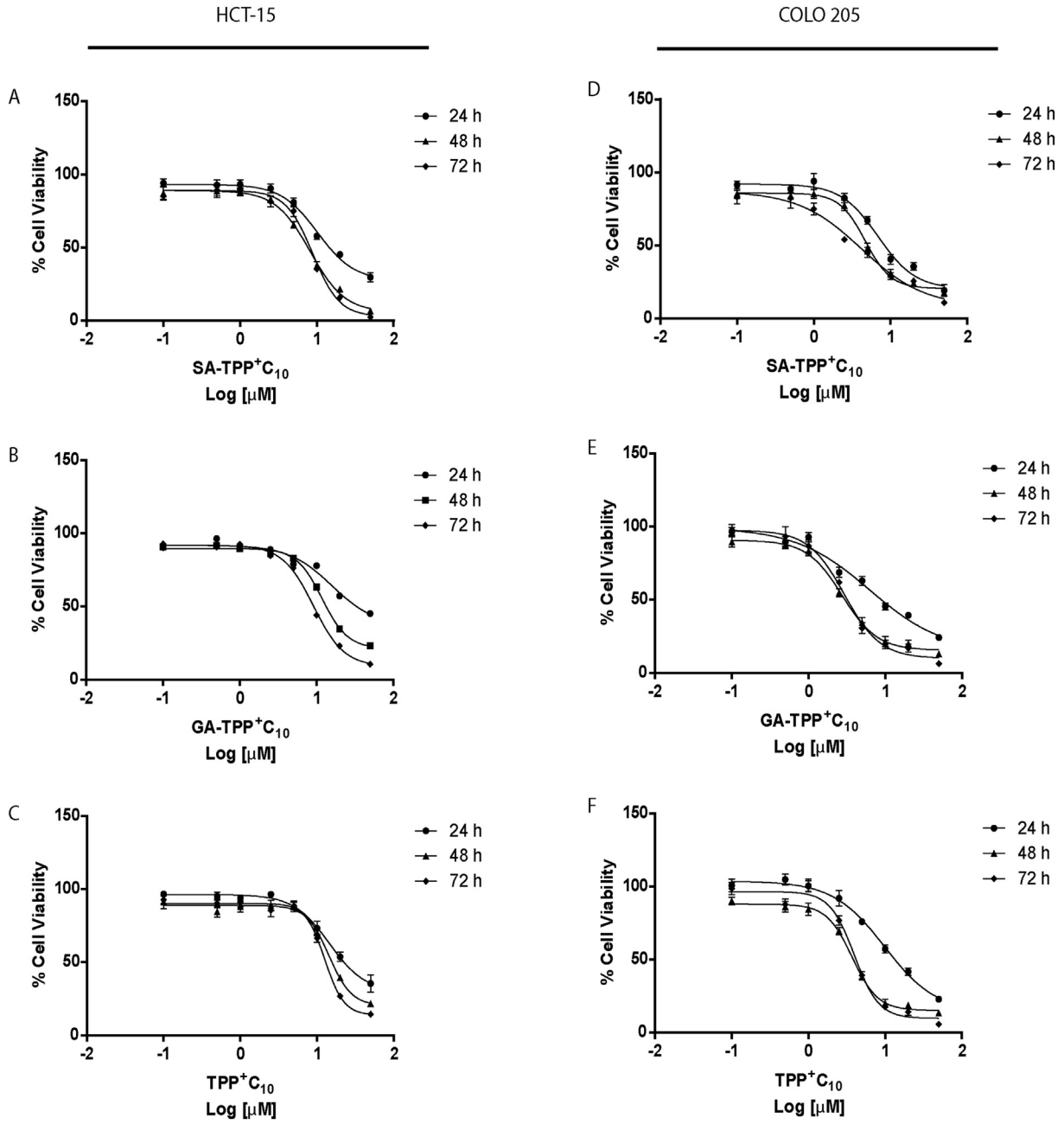

Fig. 2. Cell viability of colon cancer cell lines after exposure to benzoate-TPP^+ compounds.
The MTT assay was performed at various incubation times (24, 48, and 72 h). A), B), And C) are sigmoidal dose-response curves (variable slope), providing a graphical representation of the cytotoxicity of SA-TPP^+C_{10}, GA-TPP^+C_{10}, and TPP^+C_{10} in HCT-15 cells, respectively. D), E), And F) are sigmoidal dose-response curves for the benzoate-TPP^+ compounds SA-TPP^+C_{10}, GA-TPP^+C_{10}, and TPP^+C_{10} in COLO 205 cells, respectively. The values represent the mean of at least three independent experiments ± SD. Each assay was performed in triplicate.

although these were estimated to have a larger number of mitochondria compared to tumour cells (Fig. 3J-K).

Additionally, as a direct consequence of the uncoupling effect on OXPHOS, the electron transport chain detached from ATP synthesis. We measured intracellular ATP levels. HCT-15 and COLO 205 cells were incubated with various concentrations of each compound. Fig. 4C shows that the compounds decreased ATP levels in the HCT-15 cell line. Both SA-TPP^+C_{10} and GA-TPP^+C_{10} induced a significant decrease in ATP levels at concentrations above 20 μM, while TPP^+C_{10} only produced a modest albeit significant reduction above 30 μM. Similar results were observed in COLO 205 cells (Fig. 4D) without affecting cell viability (Fig. S4A—F). To evaluate the impact of the decreased intracellular ATP levels, we also evaluated the activity phosphorylation of the essential metabolic sensor AMPK (AMP-activated protein kinase). We used 20 μM SA-TPP^+C_{10}, GA-TPP^+C_{10} and TPP^+C_{10} for this experiment, a concentration at which a significant decrease in ATP level was observed in both CRC cell lines after 4 h of incubation. Fig. 4E and F show the results for AMPK phosphorylation induced by all benzoate-TPP^+ derivatives after 4 h of incubation in HCT-15 and COLO 205 cell lines, respectively, compared to control values.

The results suggest that the uncoupling effect of benzoate-TPP^+ compounds induces a loss of $\Delta\Psi m$, leading to decreased cellular ATP synthesis and activation of AMPK related to energetic imbalance; these early events are associated with the induction of apoptosis and cellular death.

Table 1
Cytotoxicity and selectivity of benzoate-TPP$^+$ compounds in the colon cancer cell lines HCT-15 and COLO 205.

IC_{50} = concentration necessary to achieve 50% toxicity in the cell culture after 24, 48, or 72 h of treatment. Values were calculated from the respective sigmoidal dose-response curves, representing the mean ± SD values of at least three independent experiments. Each assay was performed in triplicate.

IC_{50} values (μM) for benzoates-TPP$^+$ derivatives and control molecules in colorectal cancer cells

Compound	24 h		48 h			72 h		
	HCT-15	COLO205	HCT-15	COLO205	CCD841 (non-tumour cell line)	HCT15	COLO205	CCD841 (non-tumour cell line)
SA-TPP$^+$C$_{10}$	10.90 ± 1.24	5.8 ± 0.64	8.35 ± 0.73**	4.07 ± 0.61****	27.45 ± 3.73	8.69 ± 0.82*	3.24 ± 0.83****	17.86 ± 5.94
GA-TPP$^+$C$_{10}$	13.02 ± 2.51	5.3 ± 0.49	11.32 ± 1.3****	2.77 ± 0.61****	114.72 ± 25.1 [a]	10.22 ± 0.47**	3.01 ± 0.28****	31.02 ± 13.6 [a]
TPP$^+$C$_{10}$	15.27 ± 1.06	9.54 ± 0.46	14.23 ± 1.3**	3.64 ± 0.14****	38.49 ± 7.52	12.20 ± 0.43	4.01 ± 0.57	8.24 ± 3.06
OH-C$_{10}$SA	> 200	> 200	> 200	> 200	N/A	> 200	> 200	N/A
OH-C$_{10}$GA	> 200	46,75 ± 1,58	> 200	40,60 ± 3,62	N/A	> 200	32,85 ± 5,88	N/A
OH-C$_{10}$	> 400	> 400	> 400	> 400	N/A	> 400	> 400	N/A
C$_{10}$TPP$^+$	N/A	2.24 ± 0.11	N/A	0.68 ± 0.08	N/A	0.63 ± 0.02	0.58 ± 0.10	N/A

** or **** indicate a significant difference ($p < .001$ or $p < .0001$) between tumour and non-tumour cells for a given compound. *p*-values were calculated using a two-way ANOVA and Tukey's post-hoc test.
N/A: not analyze.
[a] Indicates a significant difference ($p < .0001$) between compounds for CCD 841 CoN.

Table 2
Selectivity index for benzoates-TPP$^+$ derivatives at 48 h and 72 h.

Values were calculated from IC_{50} ratio between non-tumour cell and tumour cell lines from the respective sigmoidal dose-response curves.

Selectivity Index for benzoates-TPP+ derivatives at 48 h and 72 h

Compound	48 h		72 h	
	CCD 841 CoN/HCT-15	CCD 841 CoN/COLO 205	CCD 841 CoN/HCT-15	CCD 841 CoN/COLO 205
SA-TPP$^+$C$_{10}$	3.3	6.7	2.1	5.5
GA-TPP$^+$C$_{10}$	10.1	41.4	3.0	10.3
TPP$^+$C$_{10}$	2.7	10.6	0.68	2.1

3.4. Apoptosis induced by benzoate-TPP$^+$ compounds

Loss of ΔΨm induces cell death. This apoptotic event may occur when cytochrome C is released from the mitochondria into the cytoplasm and engages with the apoptosome to trigger the apoptosis mechanism (Kroemer et al., 2007). We previously demonstrated that the compounds studied here can induce a decrease in ΔΨm. However, it remained uncertain whether this loss of ΔΨm was pivotal in inducing apoptosis. In Fig. 5, representative dot plots show that all compounds induced apoptosis after 48 h of incubation in both the HCT-15 and COLO 205 cell lines at the assessed concentrations (Fig. 5A and B, respectively). The data show that higher concentrations of the compounds were required to induce the apoptotic effect in HCT-15 cells than in COLO 205 cells (graphical quantification). Moreover, the induction of apoptosis was measured in both cell lines at an early time point (24 h). The differences between the effects of the compounds compared to the control conditions were significant only in the COLO 205 cell line. The HCT-15 cell line showed greater resistance to the effects of the compounds (Fig. S6). Furthermore, the results showed that the compounds assessed did not induce apoptotic death in the non-tumour cell line (Fig. 5C). In Fig. S7, shows cell population selected for the three cell lines to measure the apoptosis death and cell debris not considered for data analysis.

Fig. 6 shows that all compounds induced caspase 3 activation after 24 h of incubation in both cell lines. However, the HCT-15 cell line (Fig. 6A) showed more resistance to this caspase activation than the COLO 205 cell line (Fig. 6B).

The results suggest that benzoate-TPP$^+$ derivatives are capable of inducing apoptosis, an event that occurs after the onset of the uncoupling effect and the decrease in ΔΨm. In spite of the resistance of the HCT-15 cell line to apoptotic death, the compounds may be able to induce apoptosis at increased concentrations of the drug.

4. Discussion

4.1. Hydroxybenzoic acid derivatives produce cytotoxic effects in tumour cells

Several recent reports have provided evidence of the cytotoxic activity of gallic acid (GA), a polyphenolic compound found in many foods common to the Mediterranean diet. GA has antioxidant effects in many types of cells, as well as a broad range of biological activities, including anticancer and anti-inflammatory properties (Inoue et al., 1995; Kim et al., 2006; Park et al., 2008). Specifically, GA alone has a selective cytotoxic effect on many human tumour cell lines, including mammary, colon (such as HCT-15 and COLO 205), and prostate (Inoue et al., 1995; Russell Jr. et al., 2012; Salucci et al., 2002; Subramanian et al., 2016). However, the effects of GA alone have been documented in vitro at high concentrations, which are difficult to achieve in vivo (Shahrzad et al., 2001). On the other hand, several GA ester derivatives have been synthetized, showing cytotoxicity with respect to their lipophilicity and decreasing the IC_{50} value compared to GA in various tumour cell lines (Frey et al., 2007).

To improve efficacy in some pharmacophore groups and to target mitochondria, cationic molecules attached to the main structure have been shown to be a potential tool to increase the amount of drug in these organelles (Yang et al., 2016). The TPP$^+$ group may have the potential to improve the cytotoxicity and selectivity of several pharmacophore groups, such as GA esters. Moreover, TPP$^+$ is a very widely used moiety to concentrate molecules in the mitochondria, especially due to its delocalized charge between the phenyl groups present in its structure (Trendeleva et al., 2013). Our results showed that the TPP$^+$ moiety in our GA ester (TPP$^+$C$_{10}$) improves its cytotoxic effects, increasing the potency and efficacy with respect to the GA ester, as we show with a comparison of IC_{50} values (Table 1), and these concentrations may be achievable in vivo. We previously reported high TPP$^+$C$_{10}$ efficacy in vitro and in vivo in murine mammary adenocarcinoma (Jara et al., 2014; Peredo-Silva et al., 2017). Our data show that TPP$^+$C$_{10}$ produces more potent cytotoxic effects than GA in CRC cells as reported in other investigations (Subramanian et al., 2016).

Additionally, salicylic acid and gentisic acid (Fig. S2B and S2C) (mono- and dihydroxybenzoic acid, respectively) have been reported to be chemopreventive agents (Hua et al., 2019). Gentisic acid has been described as the effector of aspirin-antitumour effects in brain and

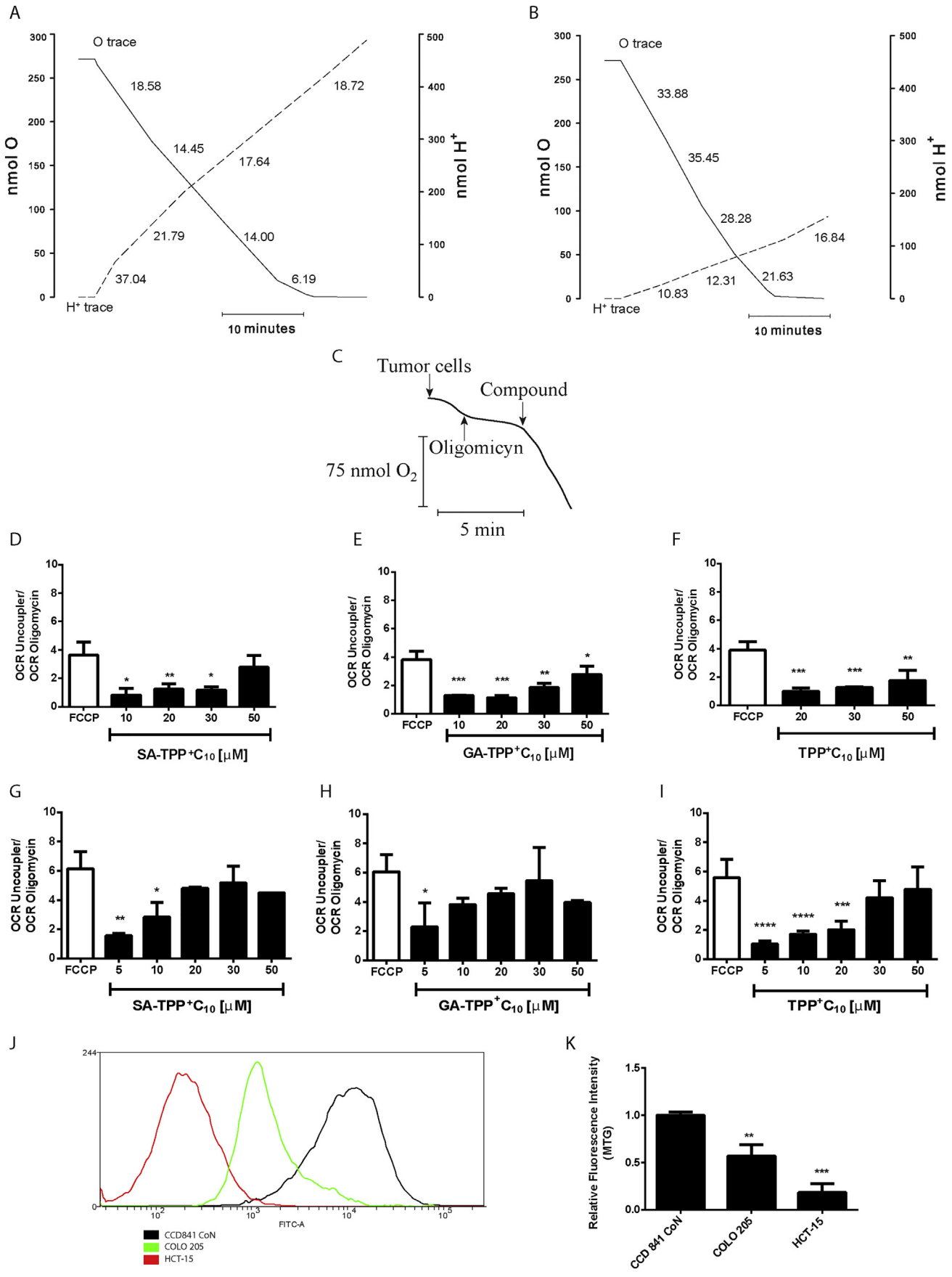

(caption on next page)

Fig. 3. Uncoupling effects of benzoate-TPP$^+$ compounds in colon cancer cell lines.
Curves A) and B) show representative traces for the baseline O_2 consumption rate (OCR) and H^+ release rate of the HCT-15 and COLO 205 cell lines, respectively. The numbers above the curve represent nmol O/min*mg protein, and the numbers under the curve represent nmol H^+/min*mg protein. The traces were fitted using SigmaPlot 12 software. C) Schematic graphic of cell respiration and procedures. D), E) And F) show the OCR of HCT-15 cells after exposure to SA-TPP$^+C_{10}$, GA-TPP$^+C_{10}$, and TPP$^+C_{10}$, respectively. G), H), And I) show the OCR of COLO 205 cells after exposure to SA-TPP$^+C_{10}$, GA-TPP$^+C_{10}$ or TPP$^+C_{10}$, respectively. The OCR in the presence of the experimental compounds was normalized to the OCR in the presence of oligomycin and is compared with the OCR in the presence of FCCP. The data shown represent the mean ± SD values of at least five independent experiments. Significant differences between the experimental conditions vs. control (FCCP) are indicated by asterisks (one-way ANOVA, Bonferroni post hoc test); *$p < .05$; **$p < .01$; ***$p < .001$; ****$p < .0001$. J) Plot of mitochondrial mass from tumour and non-tumour cells by using MitoTracker Green FM. K) Quantification of mitochondrial mass of tumour and non-tumour cell lines. The mitochondrial mass values shown represent the mean ± SD of three independent experiments. The data were normalized to the non-tumour cells (CCD 841 CoN). Significant differences between the tumour and non-tumour cells are indicated by asterisks (one-way ANOVA, Bonferroni's post hoc test); **$p < .01$; ***$p < .001$.

breast cancer, with a non-specified target (Altinoz et al., 2018). Otherwise, both acids alone have been described as CDK inhibitors in CRC, but at higher concentrations (200–300 μM) (Dachineni et al., 2017). Our results showed that mono- and dihydroxy benzoate-TPP$^+$ derivatives from salicylic and gentisic acid (SA-TPP$^+C_{10}$ and GA-TPP$^+C_{10}$, respectively) produce similar cytotoxicity to the trihydroxy benzoic derivative (TPP$^+C_{10}$) in HCT-15 and COLO 205 cells, and these effects were more potent than the ester derivatives without TPP$^+$ moiety (Table 1). Altogether, our data reveal that TPP$^+$ improves the cytotoxic effects with respect to the acids and esters, comparing our results with the previously described potencies of salicylic and gentisic acids.

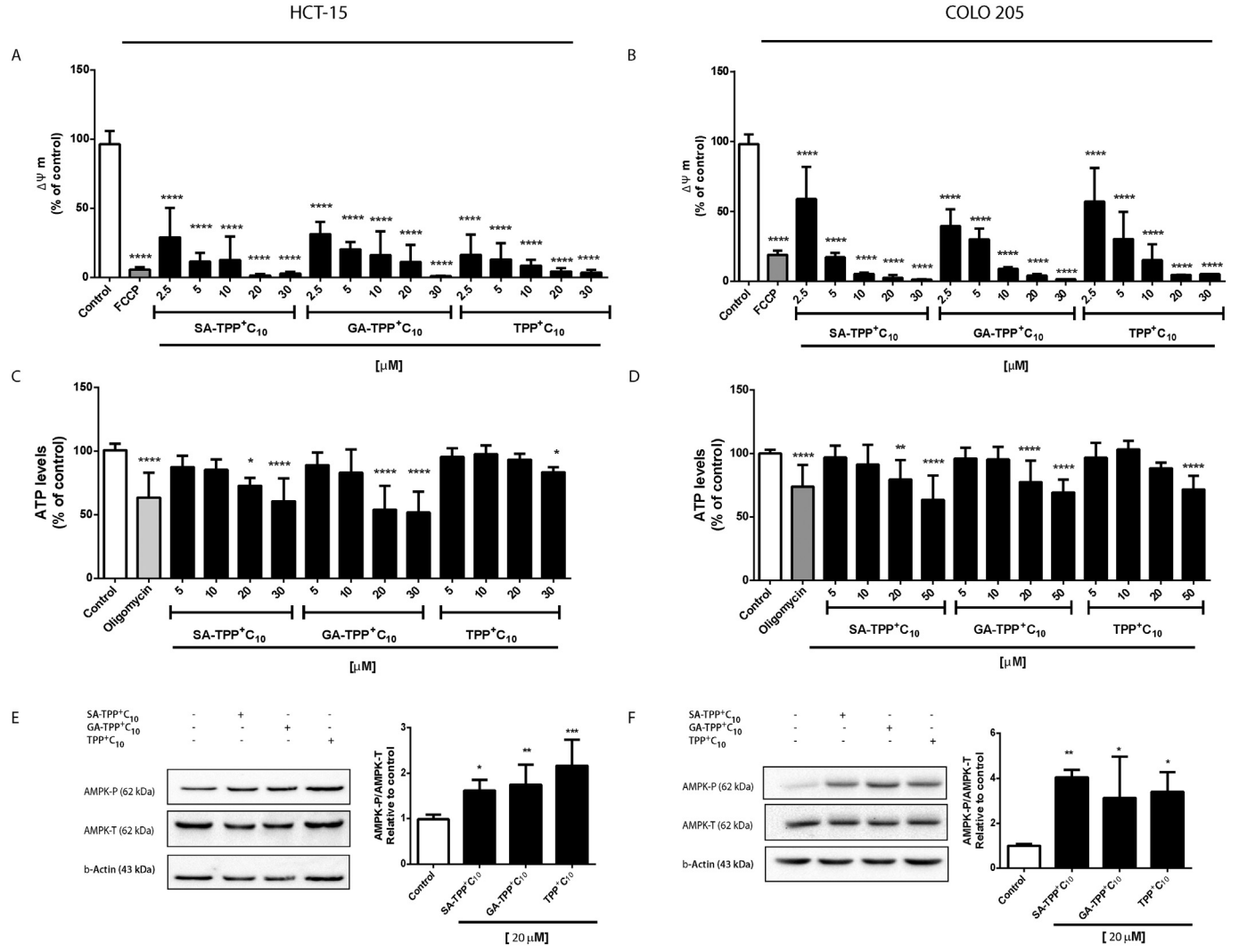

Fig. 4. Metabolic alterations produced by benzoate-TPP$^+$ compounds in colon cancer cell lines.
The effects of various concentrations of SA-TPP$^+C_{10}$, GA-TPP$^+C_{10}$, and TPP$^+C_{10}$ on ΔΨm were measured using a TMRM probe, sensitive to mitochondrial-transmembrane potential, after 30 min of incubation with the compounds in A) HCT-15 and B) COLO 205 cells. The data showed the dissipation of intensity of the TMRM probe, signal of mitochondrial potential loss. The data were normalized to the control values. The ΔΨm values shown represent the mean of four independent experiments ± SD. Besides, effects of various concentrations of SA-TPP$^+C_{10}$, GA-TPP$^+C_{10}$, and TPP$^+C_{10}$ after 4 h of incubation on intracellular ATP levels, measured by CellTiter-Glo Luminescent Assay, in C) HCT-15 and D) COLO 205 cells. The values showed the average ATP levels for each condition and the comparison with the control. Finally, AMPK phosphorylation induced by each compound (20 μM) after 4 h of treatment was evaluated using western blot analysis in E) HCT-15 and F) COLO 205 cells. The AMPK-P and AMPK-T values shown represent the mean of five independent experiments. Significant differences between the experimental conditions and control are indicated by asterisks (one-way ANOVA, Bonferroni post hoc test); *$p < .05$; **p < .01; ***p < .001; ****$p < .0001$.

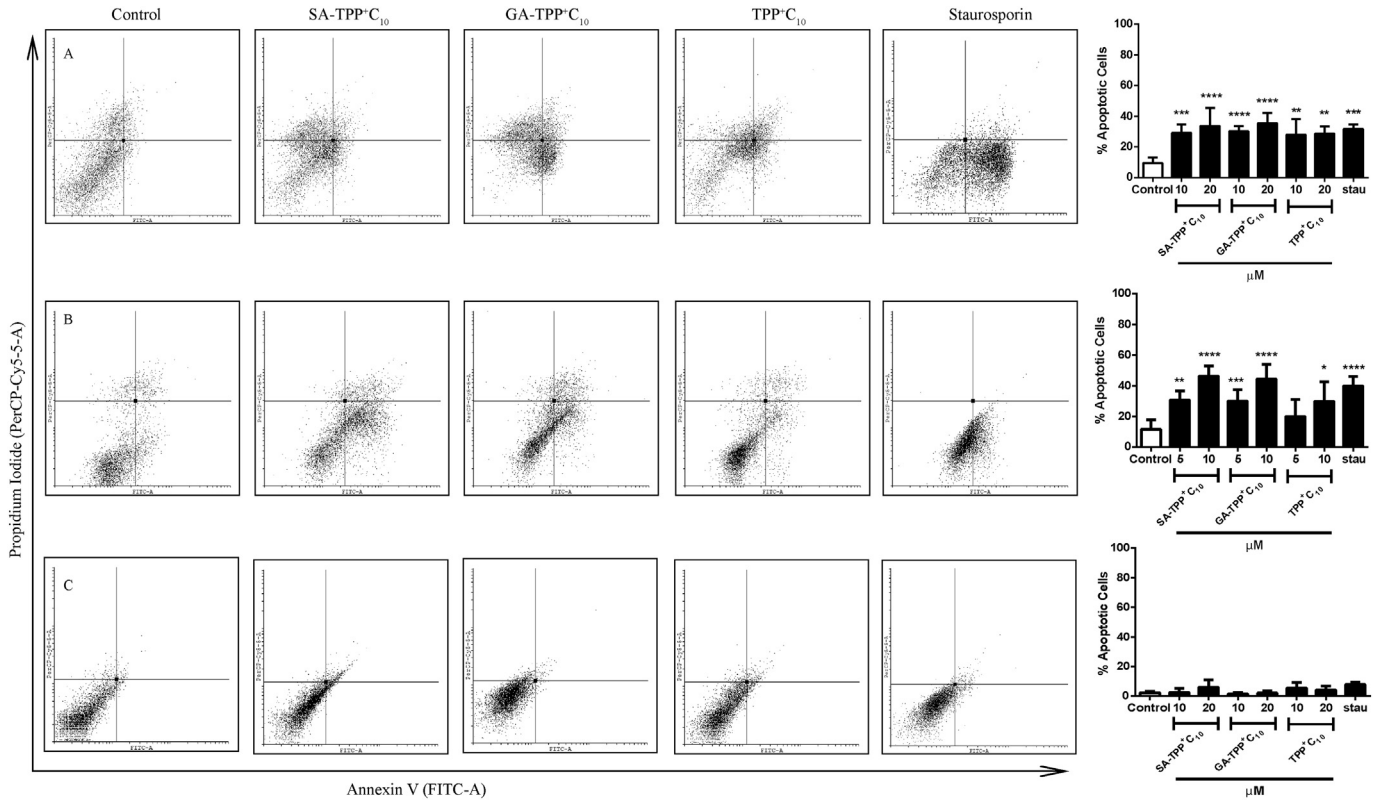

Fig. 5. Benzoate-TPP$^+$ compounds induce apoptosis in colon cancer cell lines.
Apoptosis levels induced by the compounds after 48 h of incubation were assessed in HCT-15, COLO 205 and CCD841 CoN cell lines. Representative scatterplots of higher concentrations tested are shown for A) HCT-15 and B) COLO 205C) CCD841 CoN cells. Apoptosis measurement quantifications are graphically HCT-15, D) COLO 205. Assessments were performed using Cyflogic software (version 1.2.1). Staurosporine (STS; 10 µM) was used as a positive apoptosis-induction control. Apoptosis was assessed by quantifying Annexin V-FITC positive cells using flow cytometry (FACS Canto A, BD Biosciences). The data shown represent the mean ± SD of four independent experiments. Significant differences between the experimental conditions and the control are indicated by asterisks (one-way ANOVA, Bonferroni's post hoc test); *p < .05; **p < .01; ***p < .001; ****p < .0001.

Moreover, the results suggest that GA-TPP$^+$C$_{10}$ has a higher selectivity for tumour cells than TPP$^+$C$_{10}$ or SA-TPP$^+$C$_{10}$ (Table 2). Higher concentrations of all of the compounds assessed were required to produce cytotoxic effects in non-tumour cells (Table 1, Fig. S2).

4.2. Benzoate-TPP$^+$ derivatives targeting mitochondria

The cytotoxic effects of GA and its esters are induced through the generation of reactive oxygen species (ROS) and the inhibition of the electron transport chain complex (Chen et al., 2009; Frey et al., 2007). In this study, we show that conjugation of a GA ester with TPP$^+$ confers the ability to induce mitochondrial uncoupling (Fig. 2) without increasing ROS levels (Fig. S5A and S5B). This event represents a novel mode of action that is different than the mechanisms previously described for GA or GA esters (Chen et al., 2009; Frey et al., 2007). These uncoupling effects can be explained by the protonophore characteristics of the hydroxy groups present on the phenyl rings of GA. These hydroxy groups are protonated on the outer side of the internal mitochondrial membrane (intermembrane space) and are deprotonated on the inner side of the internal mitochondrial membrane (matrix), according to the respective pKa values of the hydroxy groups (Sandoval-Acuna et al., 2016). This mechanism of action is also present for SA-TPP$^+$C$_{10}$ and GA-TPP$^+$C$_{10}$, showing similar uncoupling effects to TPP$^+$C$_{10}$ in CRC cell lines. Therefore, the results suggest that the uncoupling effect is independent of the number of hydroxy groups present on the benzoic acid ring. In addition, mono- and dihydroxybenzoic acids are described as CDK inhibitors (Dachineni et al., 2017); however, our results in CRC cells show that esterification and TPP$^+$ incorporation into the structure may modified their mechanism of action.

The 10-carbon length of the aliphatic chain has been described as an important characteristic to penetrate the mitochondria and produce the uncoupling effect. These data are consistent with findings from Antonenko and colleagues (Antonenko et al., 2016), who reported that fluorescein linked to TPP$^+$ with a 10-carbon aliphatic chain induces the uncoupling of OXPHOS, decreasing ROS and providing a neuroprotective effect in trauma models (Antonenko et al., 2016; Denisov et al., 2014). Interestingly, the aliphatic chain attached to TPP$^+$ alone, without the pharmacophore group (DA-TPP$^+$), has higher cytotoxicity than benzoate-TPP$^+$ compounds (Table 1, Fig. S1G). However, this compound induces necrotic cell death and targets tumour and non-tumour cells in a nonspecific manner, as shown in our results and those results previously reported by our group in breast tumour cells (Sandoval-Acuna et al., 2016). Moreover, the lack of a TPP$^+$ moiety on the benzoate with 10-carbon aliphatic chain derivatives (OH-C$_{10}$, OH-C$_{10}$GA and OH-C$_{10}$SA) reduces the potency and efficacy of the pharmacophore group, suggesting a decrease in the mitochondrial target. Further experiments may be performed to confirm this affirmation.

4.3. Benzoate-TPP$^+$ derivatives act independent of cellular metabolism

Our data show similar cytotoxic results for each of the benzoate TPP$^+$ derivatives in the CRC lines, independent of cell metabolic characteristics, for both glycolytic and oxidative behaviours (Fig. 3A and B). We show that HCT-15 cells behave as a glycolytic cell type. This result is consistent with the finding that HCT-15 cells show significantly greater rates of proton production at baseline than the COLO 205 cells. In contrast, the HCT-15 cells show a lower cellular respiration rate than the COLO 205 cells, which seems to rely more on functional oxidative

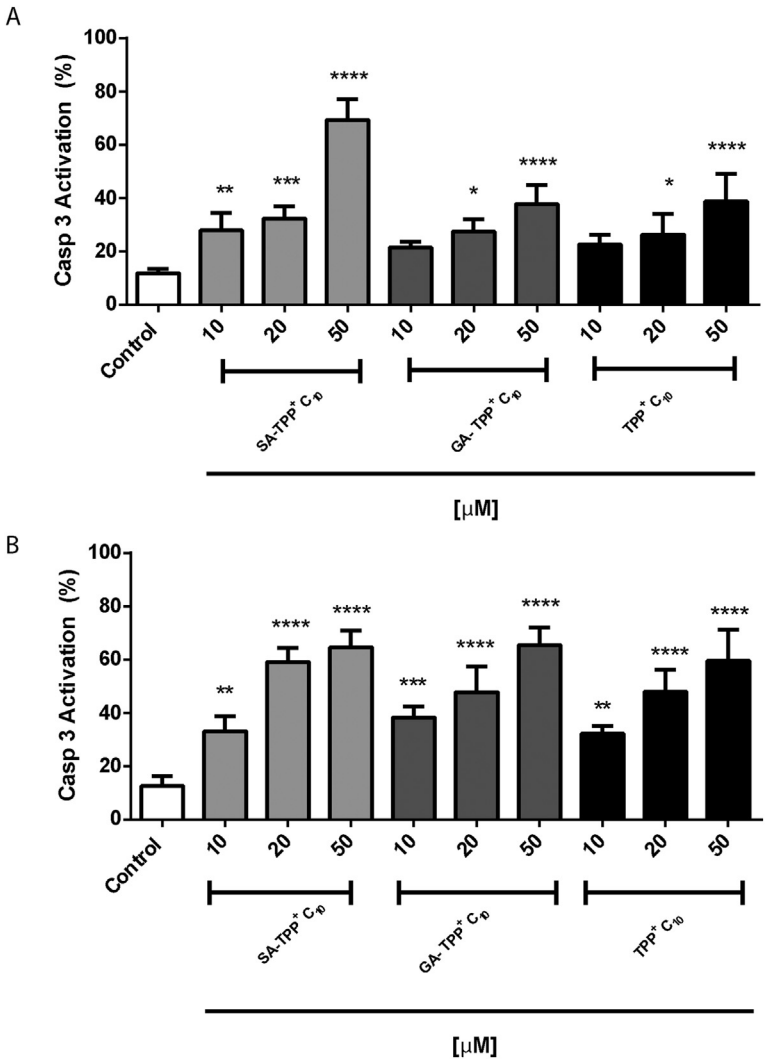

Fig. 6. Benzoate-TPP^+ compounds induce the activation of caspase 3. Compound-induced caspase 3 activation after 24 h of incubation was assessed in A) HCT-15 and B) COLO 205 cell lines using PE anti-caspase 3 antibody. Assessments were performed using Cyflogic software (version 1.2.1). Staurosporine (STS; 10 μM) was used as a caspase 3-induction control. Caspase 3 activation was assessed by quantifying PE-positive cells using flow cytometry (FACS Canto, BD Biosciences). The data shown represent the mean ± SD of four independent experiments. Significant differences between the experimental conditions and the control are indicated by asterisks (one-way ANOVA, Bonferroni's post hoc test); *p < .05; **p < .01; ***p < .001; ****p < .0001.

phosphorylation. It has been reported that metastatic cells present more mitochondrial mass and OXPHOS activity surrounded by a glycolytic environment that has mitochondrial dysfunction and loss of mitochondrial mass, which is associated with drug resistance (Sotgia et al., 2012). Moreover, the increased drug resistance has been suggested to be the result of less mitochondrial DNA. We showed that the HCT-15 cell line has a significantly lower mitochondrial mass than the COLO 205 cell line (Fig. 3J-K), which may partly explain the slight resistance of the HCT-15 cell line to our compounds, which likely influences drug targeting. However, these molecules can generate a potent cytotoxic effect despite the glycolytic behaviours of the cells. Altogether, our data suggest that the three compounds are able to induce tumour cell death regardless of the metabolic features of each type of cell, which is in agreement with our previous results in breast cancer cells (Sandoval-Acuna et al., 2016). In this sense, the compounds showed similar effects and selectivity in CRC cells when compared to murine and human breast cancer cells, leading to the speculation that these new molecules are nonspecific among tumour cell lines and have a high selectivity for them, and the principal feature involved is the mitochondrial differences in cancer cells.

4.4. Benzoate-TPP^+ derivatives induce apoptotic death by mitochondrial stress

As a direct consequence of this mitochondrial disturbance produced by the uncoupling effect, ΔΨm and ATP levels are reduced. These changes trigger an increased AMP/ATP ratio, which activates AMPK phosphorylation, a pivotal metabolic sensor (Lim et al., 2009; Sergent et al., 2002). Our results are in agreement with this mechanism, which implies that our compounds (SA-TPP^+C_{10}, GA-TPP^+C_{10} and TPP^+C_{10}) are able to reach the mitochondria and induce an uncoupling effect, which triggers the collapse of the function of these organelles, causes them enter metabolic stress, decreases cellular ATP levels, and leads the cells to apoptosis.

It should be noted that while the IC_{50} values in HCT-15 cells were higher than in COLO 205 cells (Table 1, 8–15 in HCT-15 cells), these values are still much lower than the IC_{50} value for 5-FU, a classical CRC drug treatment (47.5 μM), in this cell line (Bracht et al., 2010). In addition, our own results showed that 5-FU induces cytotoxic effects in COLO 205 cells with a higher IC_{50} than our compounds (Fig. S8), suggesting that SA-TPP^+C_{10}, GA-TPP^+C_{10} and TPP^+C_{10} are improved molecules, inducing cell death selectivity compared with a classical treatment for CRC.

On the other hand, the compounds did not induce a loss in ΔΨm or apoptosis (Fig. S2G and Fig. 5E) in non-tumour cells. These results confirm the higher selectivity of these compounds for tumour cells vs. normal cells.

5. Conclusion

Our results show that benzoate-derivative compounds show potential as anti-colorectal cancer drugs, operating through different modes

of action than the current therapies for this disease. These new molecules selectively target mitochondria with high potency and efficacy, inducing the uncoupling of oxidative phosphorylation, which in turn triggers apoptotic cell death. The mechanism of action of these compounds is associated with the TPP^+ moiety added to the pharmacophore, which produces mitochondrial tropism. The benzoic acid derivatives studied here are promising candidates for assessing in vivo models of CRC.

Supplementary data to this article can be found online at https://doi.org/10.1016/j.tiv.2020.104814.

Ethics approval and consent to participate

Not applicable.

Consent to publish

Not applicable.

Availability of data and materials

Not applicable. Our manuscript did not contain any data.

Funding

This work was supported by the following grants from the Consejo Nacional de Ciencia y Tecnología (CONICYT: FONDECYT 11160281 (MC), FONDECYT 1180296 (JF), FONDECYT 1130189 (JDM), the Academy Insertion Grant 791220004 (MC-JAJ); from the Vicerrectoría de Investigación y Desarrollo, Universidad de Chile (Enlace ENL022/16) (JF).

The grants CONICYT: FONDECYT 11160281 (MC) and the Academy Insertion Grant 791220004 allowed the development of the project, permeating the purchase of supplies and cell lines, the design of the study and collection, analysis, and interpretation of data.

The grants FONDECYT 1180296 (JF), FONDECYT 1130189 (JDM) and Universidad de Chile (Enlace ENL022/16) (JF) allowed the operation of the laboratory and the writing and revision of the manuscript.

Authors contributions

J.A.J., M.C, and J.F. designed the study, analysed the data, and wrote the manuscript. J.A.J., D.R., M.P., M.C. and J. F. performed the experimental work. V.C.C. performed the organic synthesis. S.F.R., C.S.A., E.P. and J.D.M. contributed to project development and data interpretation.

We declare that all authors have read and approved the manuscript.

Declaration of Competing Interest

The authors declare no competing financial interest.

Acknowledgements

This work was supported by the following grants from the Consejo Nacional de Ciencia y Tecnología (CONICYT: FONDECYT 11160281 (MC), FONDECYT 1180296 (JF), FONDECYT 1130189 (JDM), the Academy Insertion Grant 791220004 (MC-JAJ)); from the Vicerrectoría de Investigación y Desarrollo, Universidad de Chile (Enlace ENL022/16) (JF).

References

Altinoz, M.A., Elmaci, I., Cengiz, S., Emekli-Alturfan, E., Ozpinar, A., 2018. From epidemiology to treatment: Aspirin's prevention of brain and breast-cancer and cardioprotection may associate with its metabolite gentisic acid. Chem. Biol. Interact. 291, 29–39.

Antonenko, Y.N., Denisov, S.S., Silachev, D.N., Khailova, L.S., Jankauskas, S.S., Rokitskaya, T.I., Danilina, T.I., Kotova, E.A., Korshunova, G.A., Plotnikov, E.Y., Zorov, D.B., 2016. A long-linker conjugate of fluorescein and triphenylphosphonium as mitochondria-targeted uncoupler and fluorescent neuro- and nephroprotector. Biochim. Biophys. Acta 1860, 2463–2473.

Bracht, K., Nicholls, A.M., Liu, Y., Bodmer, W.F., 2010. 5-fluorouracil response in a large panel of colorectal cancer cell lines is associated with mismatch repair deficiency. Br. J. Cancer 103, 340–346.

Chen, H.M., Wu, Y.C., Chia, Y.C., Chang, F.R., Hsu, H.K., Hsieh, Y.C., Chen, C.C., Yuan, S.S., 2009. Gallic acid, a major component of Toona sinensis leaf extracts, contains a ROS-mediated anti-cancer activity in human prostate cancer cells. Cancer Lett. 286, 161–171.

Cordano, G., Pezoa, J., Munoz, S., Rivera, E., Medina, J., Nunez-Vergara, L.J., Pavani, M., Guerrero, A., Ferreira, J., 2002. Inhibitory effect of vanillin-like compounds on respiration and growth of adenocarcinoma TA3 and its multiresistant variant TA3-MTX-R. Eur. J. Pharm. Sci. 16, 255–263.

Dachineni, R., Kumar, D.R., Callegari, E., Kesharwani, S.S., Sankaranarayanan, R., Seefeldt, T., Tummala, H., Bhat, G.J., 2017. Salicylic acid metabolites and derivatives inhibit CDK activity: novel insights into aspirin's chemopreventive effects against colorectal cancer. Int. J. Oncol. 51, 1661–1673.

Denisov, S.S., Kotova, E.A., Plotnikov, E.Y., Tikhonov, A.A., Zorov, D.B., Korshunova, G.A., Antonenko, Y.N., 2014. A mitochondria-targeted protonophoric uncoupler derived from fluorescein. Chem. Commun. (Camb.) 50, 15366–15369.

Frey, C., Pavani, M., Cordano, G., Munoz, S., Rivera, E., Medina, J., Morello, A., Diego Maya, J., Ferreira, J., 2007. Comparative cytotoxicity of alkyl gallates on mouse tumor cell lines and isolated rat hepatocytes. Comp. Biochem. Physiol. A Mol. Integr. Physiol. 146, 520–527.

Granci, V., Cai, F., Lecumberri, E., Clerc, A., Dupertuis, Y.M., Pichard, C., 2013. Colon cancer cell chemosensitisation by fish oil emulsion involves apoptotic mitochondria pathway. Br. J. Nutr. 109, 1188–1195.

Hoye, A.T., Davoren, J.E., Wipf, P., Fink, M.P., Kagan, V.E., 2008. Targeting mitochondria. Acc. Chem. Res. 41, 87–97.

Hua, H., Zhang, H., Kong, Q., Wang, J., Jiang, Y., 2019. Complex roles of the old drug aspirin in cancer chemoprevention and therapy. Med. Res. Rev. 39, 114–145.

Inoue, M., Suzuki, R., Sakaguchi, N., Li, Z., Takeda, T., Ogihara, Y., Jiang, B.Y., Chen, Y., 1995. Selective induction of cell death in cancer cells by gallic acid. Biol. Pharm. Bull. 18, 1526–1530.

Jara, J.A., Castro-Castillo, V., Saavedra-Olavarria, J., Peredo, L., Pavanni, M., Jana, F., Letelier, M.E., Parra, E., Becker, M.I., Morello, A., Kemmerling, U., Maya, J.D., Ferreira, J., 2014. Antiproliferative and uncoupling effects of delocalized, lipophilic, cationic gallic acid derivatives on cancer cell lines. Validation in vivo in singenic mice. J. Med. Chem. 57, 2440–2454.

Kalyanaraman, B., Cheng, G., Hardy, M., Ouari, O., Sikora, A., Zielonka, J., Dwinell, M.B., 2017. Modified metformin as a more potent anticancer drug: mitochondrial inhibition, redox Signaling, Antiproliferative effects and future EPR studies. Cell Biochem. Biophys. 75, 311–317.

Khelwatty, S.A., Essapen, S., Seddon, A.M., Fan, Z., Modjtahedi, H., 2015. Acquired resistance to anti-EGFR mAb ICR62 in cancer cells is accompanied by an increased EGFR expression, HER-2/HER-3 signalling and sensitivity to pan HER blockers. Br. J. Cancer 113, 1010–1019.

Kim, S.H., Jun, C.D., Suk, K., Choi, B.J., Lim, H., Park, S., Lee, S.H., Shin, H.Y., Kim, D.K., Shin, T.Y., 2006. Gallic acid inhibits histamine release and pro-inflammatory cytokine production in mast cells. Toxicol. Sci. 91, 123–131.

Kroemer, G., Galluzzi, L., Brenner, C., 2007. Mitochondrial membrane permeabilization in cell death. Physiol. Rev. 87, 99–163.

Lim, H.W., Lim, H.Y., Wong, K.P., 2009. Uncoupling of oxidative phosphorylation by curcumin: implication of its cellular mechanism of action. Biochem. Biophys. Res. Commun. 389, 187–192.

Millard, M., Pathania, D., Shabaik, Y., Taheri, L., Deng, J., Neamati, N., 2010. Preclinical evaluation of novel triphenylphosphonium salts with broad-spectrum activity. PLoS One 5.

Mirone, G., Shukla, A., Marfe, G., 2016. Signaling mechanisms of resistance to EGFR- and anti-Angiogenic inhibitors cancer. Crit. Rev. Oncol. Hematol. 97, 85–95.

Moreno-Sanchez, R., Rodriguez-Enriquez, S., Marin-Hernandez, A., Saavedra, E., 2007. Energy metabolism in tumor cells. FEBS J. 274, 1393–1418.

Murphy, M.P., 2008. Targeting lipophilic cations to mitochondria. Biochim. Biophys. Acta 1777, 1028–1031.

Neuzil, J., Dong, L.F., Rohlena, J., Truksa, J., Ralph, S.J., 2013. Classification of mitocans, anti-cancer drugs acting on mitochondria. Mitochondrion 13, 199–208.

Okada, T., Tanaka, K., Kawachi, H., Ito, T., Nishikage, T., Odagaki, T., Zarate, A.J., Kronberg, U., Lopez-Kostner, F., Karelovic, S., Flores, S., Estela, R., Tsubaki, M., Uetake, H., Eishi, Y., Kawano, T., 2016. International collaboration between Japan and Chile to improve detection rates in colorectal cancer screening. Cancer 122, 71–77.

Park, W., Chang, M.S., Kim, H., Choi, H.Y., Yang, W.M., Kim, D.R., Park, E.H., Park, S.K., 2008. Cytotoxic effect of gallic acid on testicular cell lines with increasing H2O2 level in GC-1 spg cells. Toxicol. in Vitro 22, 159–163.

Pavlova, N.N., Thompson, C.B., 2016. The emerging hallmarks of Cancer metabolism. Cell Metab. 23, 27–47.

Peredo-Silva, L., Fuentes-Retamal, S., Sandoval-Acuna, C., Pavani, M., Maya, J.D., Castro-Castillo, V., Madrid-Rojas, M., Rebolledo, S., Kemmerling, U., Parra, E., Ferreira, J., 2017. Derivatives of alkyl gallate triphenylphosphonium exhibit antitumor activity in a syngeneic murine model of mammary adenocarcinoma. Toxicol. Appl. Pharmacol. 329, 334–346.

Plaza, C., Pavani, M., Faundez, M., Maya, J.D., Morello, A., Becker, M.I., De Ioannes, A., Cumsille, M.A., Ferreira, J., 2008. Inhibitory effect of nordihydroguaiaretic acid and its tetra-acetylated derivative on respiration and growth of adenocarcinoma TA3 and its multiresistant variant TA3MTX-R. In Vivo 22, 353–361.

Ralph, S.J., Neuzil, J., 2009. Mitochondria as targets for cancer therapy. Mol. Nutr. Food Res. 53, 9–28.

Reily, C., Mitchell, T., Chacko, B.K., Benavides, G., Murphy, M.P., Darley-Usmar, V., 2013. Mitochondrially targeted compounds and their impact on cellular bioenergetics. Redox Biol. 1, 86–93.

Rokitskaya, T.I., Murphy, M.P., Skulachev, V.P., Antonenko, Y.N., 2016. Ubiquinol and plastoquinol triphenylphosphonium conjugates can carry electrons through phospholipid membranes. Bioelectrochemistry 111, 23–30.

Russell Jr., L.H., Mazzio, E., Badisa, R.B., Zhu, Z.P., Agharahimi, M., Oriaku, E.T., Goodman, C.B., 2012. Autoxidation of gallic acid induces ROS-dependent death in human prostate cancer LNCaP cells. Anticancer Res. 32, 1595–1602.

Salucci, M., Stivala, L.A., Maiani, G., Bugianesi, R., Vannini, V., 2002. Flavonoids uptake and their effect on cell cycle of human colon adenocarcinoma cells (Caco2). Br. J. Cancer 86, 1645–1651.

Sandoval-Acuna, C., Fuentes-Retamal, S., Guzman-Rivera, D., Peredo-Silva, L., Madrid-Rojas, M., Rebolledo, S., Castro-Castillo, V., Pavani, M., Catalan, M., Maya, J.D., Jara, J.A., Parra, E., Calaf, G.M., Speisky, H., Ferreira, J., 2016. Destabilization of mitochondrial functions as a target against breast cancer progression: role of TPP (+)-linked-polyhydroxybenzoates. Toxicol. Appl. Pharmacol. 309, 2–14.

Sergent, C., Franco, N., Chapusot, C., Lizard-Nacol, S., Isambert, N., Correia, M., Chauffert, B., 2002. Human colon cancer cells surviving high doses of cisplatin or oxaliplatin in vitro are not defective in DNA mismatch repair proteins. Cancer Chemother. Pharmacol. 49, 445–452.

Shahrzad, S., Aoyagi, K., Winter, A., Koyama, A., Bitsch, I., 2001. Pharmacokinetics of gallic acid and its relative bioavailability from tea in healthy humans. J. Nutr. 131, 1207–1210.

Sotgia, F., Whitaker-Menezes, D., Martinez-Outschoorn, U.E., Flomenberg, N., Birbe, R.C., Witkiewicz, A.K., Howell, A., Philp, N.J., Pestell, R.G., Lisanti, M.P., 2012. Mitochondrial metabolism in cancer metastasis: visualizing tumor cell mitochondria and the "reverse Warburg effect" in positive lymph node tissue. Cell Cycle 11, 1445–1454.

Subramanian, A.P., Jaganathan, S.K., Mandal, M., Supriyanto, E., Muhamad, I.I., 2016. Gallic acid induced apoptotic events in HCT-15 colon cancer cells. World J. Gastroenterol. 22, 3952–3961.

Trendeleva, T.A., Sukhanova, E.I., Rogov, A.G., Zvyagilskaya, R.A., Seveina, I.I., Ilyasova, T.M., Cherepanov, D.A., Skulachev, V.P., 2013. Role of charge screening and delocalization for lipophilic cation permeability of model and mitochondrial membranes. Mitochondrion 13, 500–506.

Wahdan-Alaswad, R., Fan, Z., Edgerton, S.M., Liu, B., Deng, X.S., Arnadottir, S.S., Richer, J.K., Anderson, S.M., Thor, A.D., 2013. Glucose promotes breast cancer aggression and reduces metformin efficacy. Cell Cycle 12, 3759–3769.

Warburg, O., Wind, F., Negelein, E., 1927. The metabolism of tumors in the body. J. Gen. Physiol. 8, 519–530.

Yang, Y., Karakhanova, S., Hartwig, W., D'Haese, J.G., Philippov, P.P., Werner, J., Bazhin, A.V., 2016. Mitochondria and mitochondrial ROS in Cancer: novel targets for anticancer therapy. J. Cell. Physiol. 231, 2570–2581.

Yasui, H., Yamamoto, K., Suzuki, M., Sakai, Y., Bo, T., Nagane, M., Nishimura, E., Yamamori, T., Yamasaki, T., Yamada, K.I., Inanami, O., 2017. Lipophilic triphenylphosphonium derivatives enhance radiation-induced cell killing via inhibition of mitochondrial energy metabolism in tumor cells. Cancer Lett. 390, 160–167.

Zhang, W., Zhang, S.L., Hu, X., Tam, K.Y., 2015. Targeting tumor metabolism for Cancer treatment: is pyruvate dehydrogenase kinases (PDKs) a viable anticancer target? Int. J. Biol. Sci. 11, 1390–1400.